IEEE Access
Multidisciplinary | Rapid Review | Open Access Journal

Received February 19, 2021, accepted March 22, 2021, date of publication March 30, 2021, date of current version April 8, 2021.

Digital Object Identifier 10.1109/ACCESS.2021.3069794

Experimental Demonstration of Adaptive Optics Correction of the External Aberrations for Distributed Fiber Laser Array

CHAO GENG[1,2], FAN ZOU[1,2,3], FENG LI[1,2], GUAN HUANG[1,2,3], JING ZUO[1,2,3], JIAYING LIU[1,2,3], ZHIHUA FAN[4], AND XINYANG LI[1,2]

[1]Key Laboratory on Adaptive Optics, Chinese Academy of Sciences, Chengdu 610209, China
[2]Institute of Optics and Electronics, Chinese Academy of Sciences, Chengdu 610209, China
[3]University of Chinese Academy of Sciences, Beijing 100049, China
[4]Chengdu Research Institute, Sichuan University of Arts and Science, Dazhou 635000, China

Corresponding author: Feng Li (whu_lifeng@126.com)

This work was supported by the National Natural Science Foundation of China under Grant 61675205 and Grant 62005286.

ABSTRACT A novel method of pre-compensating the phase distortions outside the fiber laser array based on active integrated wavefront sensing is proposed and demonstrated experimentally. The scheme and the working principle are introduced. Pre-compensation experiment of the fiber laser array based on a 7-element adaptive fiber optics collimator (AFOC) array with filled factor of 0.875 is presented. Residual error RMS of 0.11μm is obtained while sensing lower order aberrations of a glass plate is with initial RMS of 0.62μm. Metric of far-field power-in-the-bucket (PIB) is improved about 3.5 times after the phase distortions are pre-compensated. This method could promote the transmission efficiency of the fiber laser array in atmosphere, without limits of array scale and transmission light delay. This method would be upgraded to correct the aberrations located in the whole optical link from laser source to the target in the future. Such method would highly promote the applications of fiber laser array based systems like free space laser communication.

INDEX TERMS Fiber laser array, wavefront sensing, adaptive optics correction.

I. INTRODUCTION

Fiber laser array transmission systems have caused great interests recently in applications like free space laser communication [1]–[5]. As a tiled array to accomplish coherent-beam-combining (CBC), this method possesses some prominent advantages of easy heat management, extendable structure and keeping high beam quality while promoting output power [6]. Meanwhile, this system replaces common large aperture monolithic transceiver with compactly packed small size sub-apertures [7], [8]. With the help of fiber-integrated electrical fiber phase modulator, ultrafast manipulating the sub-aperture phase provides better adaptive optics (AO) abilities under moderate-to-strong turbulence when compared with conventional AO enhanced beam director (BD) systems [9], [10]. Numerous indoor CBC experiments correcting array's internal phase distortions have been demonstrated [11]–[13]. Most of these results are aimed at obtaining high output power which is limited by single fiber laser's mode instability and thermal effects [14]. However, realization of CBC at the far-field target surface is more important in engineering applications [15]. Then correcting the aberrations located on the transmission path is required, especially dynamic aberrations induced by turbulence.

For higher intensity concentration of the far-field pattern, the fiber laser array is densely packed to form high filled-factor and less far-field sidelobe power [8]. Most of previous researches adopt blind optimization control to correct the external turbulence aberrations. In this control model, target-in-the-loop (TIL) [16] is utilized to get the PIB metric which is defined as the power located in a circular region on the target and expresses the concentration of energy. Gradient descent optimization algorithms, like stochastic parallel gradient descent (SPGD) [17] and single frequency dithering method [6], iteratively compute the compensation values of sub-aperture averaged pistons and tip/tilts to maximize the PIB metric. A CBC experiment of a 21-element fiber laser array over distance of 7 km with modified SPGD algorithm [18] has been reported. The fiber-integrated phase modulator with bandwidth larger than hundred kHz is verified.

The associate editor coordinating the review of this manuscript and approving it for publication was Hasan S. Mir.

TIL could work with non-cooperative targets even in distance of dozens of kilometers which is not the far field for the future large array system, where the laser array needs to work under in a conformal way. However, the potential problems in the TIL-based optimization control loop are still unresolved. Firstly, the maximum theoretical effective bandwidth of TIL depends on the inherent delay, i.e. the light time-delay spent on the round trip of the transmission distance. The correction performance would decrease rapidly with the increasing of the distance, especially when the turbulence is more intense. Secondly, the control variables are multidimensional while the input metric is single. This will result in slower convergence speed when the element number of the array is enlarged. Particularly, control bandwidth of tip/tilt device is only several kHz [19]–[21], while the number of channels is twice of the array scale. Actually, the scale of fiber laser array would reach hundred elements and the whole aperture size would reach meter level in the future. This arises great challenges to current fiber laser array systems.

To avoid the disadvantages of existing optimization control, active wavefront sensing directly over the array pupil is proposed and demonstrated experimentally in article [22]. In this paper, method of pre-compensating the aberrations located outside the fiber laser array is developed and verified with experiment. Aberration pre-compensation control is common in traditional laser transmission applications with integrated AO system. The structure of the fiber laser array proposed here is with abilities of wavefront sensing and aberrations pre-compensation and illustrated in Fig. 1. Laser beacon carrying with the information of turbulence aberrations is divided by the sub-apertures and coupled into the single-mode-fibers (SMFs) of the AFOC correspondingly. Through optimizing the coupled power, sub-aperture tip/tilt is corrected and detected [23], [24]. The continuous wavefront is sensed and the sub-aperture averaged pistons are recovered [25], [26]. External pistons of the outgoing laser beams coming from the same source are pre-compensated. With the help of fiber circulators, outgoing laser beams share the same collimating optical path with the coupled laser beams and then the tip/tilts are also pre-compensated [27]. Hundred-watt-level commercial fiber circulators could be mainly utilized in low-power applications like free space laser communication presently.

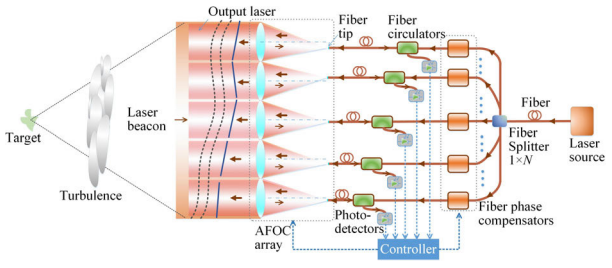

FIGURE 1. Adaptive fiber optics collimator array with active wavefront sensing and outside aberration correction.

This paper is aimed at proposing and demonstrating a new method to realize adaptive external phase distortions correction in the fiber laser array system. Based on parallel and fast control of sub-aperture tip/tilts, wavefront sensing and phase distortions' pre-compensating are achieved. Such methods would not be limited by the array scale and the transmission distance. Additionally, this adaptive correction system could be integrated in the CBC system without need of any additional mechanical or electronical devices.

II. ACTIVE PRE-COMPENSATION MODEL

Adaptive correcting the external aberrations of the distributed fiber laser array is based on active sub-aperture tip/tilts correction and detection. External aberrations like distorted wavefront brought by atmospheric turbulence are continuous and could be recovered through sub-aperture slope vector. Then the sub-aperture averaged external pistons would be detected and pre-compensated. Aberrations located in the array's whole pupil plane could be estimated as overlap of a series of Zernike modes [28]:

$$\phi(x,y)=\sum_{m=1}^{N} b_m Z_m(x,y), \tag{1}$$

where $Z_m(\cdot)$ is the Zernike mode with order of m and b_m is the Zernike coefficient. N is the recovered Zernike order number. b_m could be calculated through sub-aperture wavefront slope vector $\boldsymbol{s}$ as

$$\boldsymbol{s}=\{s_1^x, s_1^y, \ldots, s_j^x, s_j^y, \ldots, s_{N_{sub}}^x, s_{N_{sub}}^y\}, \quad j=1,\ldots,N_{sub}, \tag{2}$$

where N_{sub} is the sub-aperture number. The element S_j^x and S_j^y are written as

$$s_j^x = S_{sub}^{-1}\int_{\Omega_j}\frac{\partial\phi}{\partial x}(x,y)dxdy, \quad s_j^y = S_{sub}^{-1}\int_{\Omega_j}\frac{\partial\phi}{\partial y}(x,y)dxdy, \tag{3}$$

where $j=1,\ldots,N_{sub}$. S_{sub} is the area of each sub-aperture. Ω_j is the integral domain in the aperture plane.

Take (2) and (3) into (1), we could get

$$\boldsymbol{s}=\boldsymbol{G}\boldsymbol{b}, \tag{4}$$

where $\boldsymbol{b}$ is the Zernike coefficient vector and $\boldsymbol{b}=\{b_1, b_2, \ldots, b_m\}$. $\boldsymbol{G}$ is the transfer matrix from $\boldsymbol{b}$ to $\boldsymbol{s}$, which could be defined as

$$\boldsymbol{G}=\begin{bmatrix} G_{1,1}^x & G_{1,2}^x & \cdots & G_{1,m}^x \\ G_{1,1}^y & G_{1,2}^y & \cdots & G_{1,m}^y \\ \vdots & \vdots & \ddots & \vdots \\ G_{j,1}^x & G_{j,2}^x & \cdots & G_{j,m}^x \\ G_{j,1}^y & G_{j,2}^y & \cdots & G_{j,m}^y \\ \vdots & \vdots & \ddots & \vdots \\ G_{N_{sub},1}^x & G_{N_{sub},2}^x & \cdots & G_{N_{sub},m}^x \\ G_{N_{sub},1}^y & G_{N_{sub},2}^y & \cdots & G_{N_{sub},m}^y \end{bmatrix}, \tag{5}$$

in which the element $G^x_{j,m}$ and $G^y_{j,m}$ are written as

$$G^x_{j,m} = S^{-1}_{sub} \int_{\Omega_j} \frac{\partial Z_m}{\partial x}(x, y)dxdy,$$
$$G^y_{j,m} = S^{-1}_{sub} \int_{\Omega_j} \frac{\partial Z_m}{\partial y}(x, y)dxdy. \quad (6)$$

Actually, due to the cross coupling and aliasing in model wavefront estimation [29], larger N does not mean better recover performance. There exists an optimized recover order number N_{opt} which is less than $2N_{\text{sub}}$. In such case, (4) is an underdetermined equation and could be solved through the generalized reciprocal method. Take the inverse transformation of (4), we could get $\boldsymbol{b}$ from $\boldsymbol{s}$:

$$\boldsymbol{b} = \boldsymbol{G}^{+}\boldsymbol{s} = (\boldsymbol{G}^T\boldsymbol{G})^{-1}\boldsymbol{G}^T\boldsymbol{s}, \quad (7)$$

where $\boldsymbol{G}^+$ is the generalized inverse of $\boldsymbol{G}$ and $\boldsymbol{G}^T$ is the transpose of $\boldsymbol{G}$.

The recovered piston $\boldsymbol{P} = \{P_1, \ldots, P_j, \ldots, P_{Nsub}\}$ could be calculated as the average value of the recovered wavefront within each sub-aperture:

$$P_j = S^{-1}_{sub} \int_{\Omega_j} \phi(x, y)dxdy. \quad (8)$$

Take (7) and (1) into (8), then $\boldsymbol{P}$ could be calculated as

$$\mathbf{P} = \mathbf{D}_{TP}\boldsymbol{G}^{+}\boldsymbol{s} \quad (9)$$

where $\boldsymbol{D}_{TP}$ is the transform matrix written as

$$\boldsymbol{D}_{TP} = \begin{bmatrix} D^{1,1}_{TP} & \cdots & D^{1,k}_{TP} & \cdots & D^{1,N}_{TP} \\ \vdots & \ddots & \vdots & \ddots & \vdots \\ D^{j,1}_{TP} & \cdots & D^{j,k}_{TP} & \cdots & D^{j,N}_{TP} \\ \vdots & \ddots & \vdots & \ddots & \vdots \\ D^{N_{sub},1}_{TP} & \cdots & D^{N_{sub},k}_{TP} & \cdots & D^{N_{sub},N}_{TP} \end{bmatrix}. \quad (10)$$

The element of $\boldsymbol{D}_{TP}$ is written as

$$D^{j,k}_{TP} = S^{-1}_{sub} \int_{\Omega_j} Z_k(x, y)dxdy, \quad k = 1, \ldots, N. \quad (11)$$

When the arrangement and the structure parameters of the sub-apertures array are predetermined, $\boldsymbol{D}_{TP}\boldsymbol{G}^+$ in (9) is also decided. Then external sub-aperture pistons could be calculated through sub-aperture slope vector. Sub-aperture slope could be obtained through control of coupling the focused laser beam from space into single mode fiber [22]. It has been proved through experiments [30], [31] that sub-aperture tip/tilt phase of the outgoing laser beam could be corrected when power of coupled laser beacon from space into SMF is optimized. When the recovered pistons are loaded and pre-compensated through the fiber compensators shown in Fig. 1, the performance of the CBC of the outgoing laser beams could be further promoted. Owing to the array is sparsely arranged, the external aberrations detection is insufficient and then the aberrations correction is partial.

III. EXPERIMENTAL SETUP

The experimental setup is shown in Fig. 2. The fiber laser array is generated from a 7-element AFOC array. The AFOC array is with a hexagonal configuration, sub-aperture diameter $d = 28$ mm and adjacent sub-aperture space of 32 mm. The focal length of the collimating lens $f_c = 150$ mm. The 7 laser beams come from the same linearly polarized laser source (NKT photonics, Koheras Adjustik) at 1064 nm wavelength with power of 11 mW and line-width of 20 kHz. The source laser is divided into 8 beams by a fiber splitter. 7 of them are adopted and then pass through fiber circulators and phase compensators separately. After collimated by the lens in the AFOCs, the laser beams pass through a glass plate with diameter of 92 mm. Then the 7 laser beams are focused by a transform lens with focal length of 1.5 m. The focused beams are reflected by an electrical deflecting mirror, pass through two beam splitter prisms and then form a CBC far-field pattern. The image is magnified ten-fold by a micro-objective and then captured by a camera for monitoring. The other focused spot on the left side of splitter prism-2 is obtained by a photo-detector with a pinhole with diameter of 20 μm. Another fiber laser source with wavelength of 1064 nm and power of 2 W is placed on the right side of splitter prism-1. This linearly polarized laser shot out from the fiber tip which is placed on the focal plane formed by splitter prism-1. This laser beam is collimated by the transform lens to generate a large area laser beacon. After passing through the glass plate, this laser beacon covers the AFOC array apertures and laser located in each of the single AFOC aperture is focused and coupled into the corresponding SMF cores. The coupled beacons pass through the phase compensators (PMs) and the fiber circulators and then are finally captured by photo-detectors. The homemade PMs are with half-wave voltage of about 1.3 V and first order resonance frequency of about 32 kHz. The PMs are produced by twisting the polarization maintaining fiber around the piezoelectric ceramic ring. The processor generates voltage signals according to the coupled metrics. The voltages are amplified and drive the AFOCs to maximize the coupled metrics. As discussed in paper [23], the distorted wavefront could be recovered through the voltage values. The distorted phase we want to correct is brought by the glass plate with rough surface. Wedge angle of the glass plate should be much less than the AFOCs' deflection angle (about ± 200 μrad) or the sub-aperture tiled angle

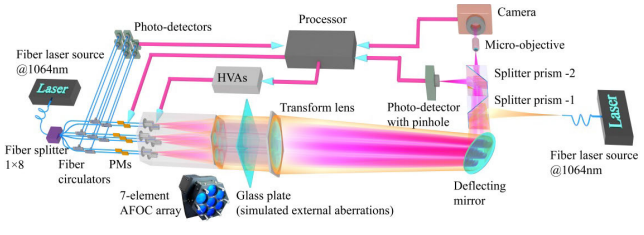

FIGURE 2. Experimental setup. HVA: High voltage amplifier. PMs: Phase compensators.

measurement would fail. The glass is carefully selected to ensure the aberrations are mainly low orders. Aberrations of Zernike orders higher than 9 would be beyond the capacity of the 7-element AFOC array sensor.

The steps of the aberrations correction are described as bellow:

Step ①: Open loop. Driving voltages applied on the AFOCs and phase compensators are set to zero. The coupled laser beam power voltages detected by the 7 photo-detectors and the PIB metric captured by the photo-detectors on the transform lens focal plane are recorded. Far-field pattern is obtained by the camera.

Step ②: Wavefront sensing calibration. The laser beacon source is collimated by the transform lens to form a plane wave beam. Voltages are applied on the AFOC to maximize the coupled beacon intensity with SPGD algorithm. Then the optical axes of the AFOCs are parallel to each other. The driving voltages remain and the values are recorded as $\boldsymbol{V}_{ts}$.

Step ③: Internal phase distortion elimination. This paper is focused on active correction of the external aberrations of the fiber laser array and then the internal phase distortions should be eliminated. This phase distortion is quasi-static and mainly caused by the fiber path length difference of the AFOCs. Here, we adopt the voltage captured by the photo-detector with pinhole placed in the focal plane of the transform lens as the CBC PIB metric. SPGD algorithm is utilized to generate the voltages applied on the phase-compensators to optimize the CBC PIB metric. The driving voltages remain and the values are recorded as $\boldsymbol{V}_{ps}$.

Step ④: Place the glass plate between the AFOC array and the transform lens. To balance the large tilt brought by the glass plate, the deflecting mirror is driven to deflect in the opposite direction.

Step ⑤: Wavefront sensing measurement. The voltages applied on AFOCs are computed iteratively from the existing voltages vector $\boldsymbol{V}_{ts}$ to maximize the coupled beacon power in each AFOC again using SPGD algorithm. Then the updated voltages remain and recorded as $\boldsymbol{V}_{te}$.

Step ⑥: Active pre-compensation of the external aberrations. From $\Delta \boldsymbol{V}_{\mathrm{t}} = \boldsymbol{V}_{te}\text{-}\boldsymbol{V}_{ts}$, we could obtain the sub-aperture wavefront slope vector $\boldsymbol{s}$ of the glass plate' phase distortion, according to paper [20]. According to formula (9), we could get the sub-aperture pistons $\boldsymbol{P}$. The scale factor between the phase change and the voltage applied on phase compensator is precisely calibrated beforehand. Then the voltages variation $\Delta \boldsymbol{V}_p$ could be calculated and voltages $\boldsymbol{V}_{ps} + \Delta \boldsymbol{V}_p$ is applied on the phase compensators.

Step ⑦: Further blind optimization. As a contrast, we adopt SPGD algorithm to further optimize the PIB metric of CBC. The voltages applied on the phase compensators are computed iteratively from the basis of $\boldsymbol{V}_{ps} + \Delta \boldsymbol{V}_p$. The convergent voltages are recorded as $\boldsymbol{V}_{pe}$.

IV. EXPERIMENTAL RESULTS AND DISCUSSION

This paper is mainly focused on how to correct the external phase distortion based on active wavefront sensing and phase pre-compensation. So, the influence of the internal phase noises in the fiber laser array should be solved in advance through certain methods. In this experiment, sub-aperture tip/tilt errors and pistons are pre-calibrated through step ② and step ③ described in part III. Internal pistons compensation could be achieved with the methods as shown in [25] and [26]. The deflection angle executed by the AFOC is decided by the driving voltage. The drift of the tip/tilt errors is negligible when the driving voltages remain.

Fig. 3(a) and 3(b) show the driving voltages curve during the internal phase distortion elimination (step ③) and further blind optimization (step ⑦) procedures correspondingly. The iterative rate in step ③ and step ⑦ is about 500 Hz. The X-axis of time begins from step ① . The driving voltages converge to certain and different values in the two courses. The embedded images are the far-field CBC patterns captured by the camera. The pattern is very similar to the ideal CBC pattern. Therefore, the sub-apertures' phase is locked in the whole pupil plane. The quasi-static pistons caused by difference of fiber path length are phased locked in Fig. 3(a). Actually, the fiber path difference is kept within several millimeters, which is much less than the coherent length of the laser source. The piston drift which accumulates during the experiment procedures is corrected in Fig. 3(b). As we can see, voltage offset after convergence in Fig. 3(a) is larger than that in Fig. 3(b). Voltage offset illustrated in Fig. 3(b) corresponds to the piston drift in about 20 seconds which may influence the experiment. The scale factor η_j between the phase change and the voltage applied on phase compensator is pre-calculated and the value is about 0.77 λ/V (λ is the wavelength and equals to 1.064 μm).

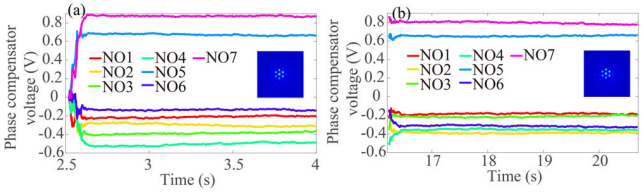

FIGURE 3. Phase compensator voltages during the phase-locking processes.

Wavefront sensing of the aberrations brought by the glass plate is based on the driving voltages deviation $\Delta \boldsymbol{V}_{\mathrm{t}}$ between step ② and step ⑤. Sub-aperture wavefront slope vector $\boldsymbol{s}$ then could be calculated and Modal wavefront recovery algorithm is utilized to recover the wavefront. The results are shown in Fig. 4 and Fig. 5. Fig. 4 illustrates the reconstruction Zernike coefficients with orders from 3 to 9. Actually, the 7-element AFOC array is similar to a scale-limited Shack-Hartmann wavefront sensor. Then only aberrations with low orders could be detected. For comparison, Zernike coefficients measured through interferometer is also listed in Fig. 4. Here, American National Standards Institute (ANSI) standard Zernike expansion is used here. It should be noticed that the coefficients of the first two Zernike modes (X-tilt and Y-tilt) are not listed here because many other issues could

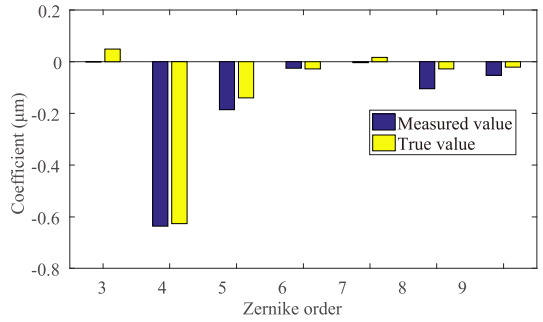

FIGURE 4. The measured Zernike coefficients with index from 3 to 9.

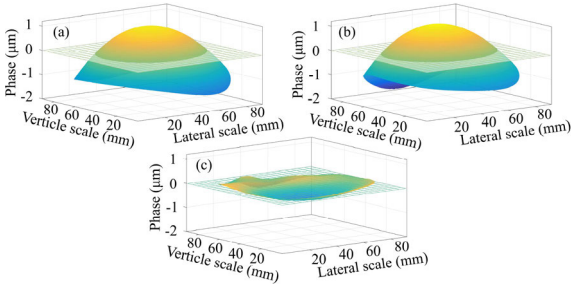

FIGURE 5. (a) Wavefront profile measured through interferometer; (b) Active wavefront sensing result; (c) Residual error of the recovery.

bring in global tilt error beyond the glass plate. The glass plate aberrations mainly consist of defocus (fourth order) and astigmatism (third and fifth order), as shown in Fig. 4 and Fig. 5(a). As Fig. 4 shows, the measured Zernike coefficients are very close to the true value. The reconstructed wavefront profile is shown in Fig. 5(b) and the residual error profile is illustrated in Fig. 5(c). Here, the root-mean-square (RMS) error is utilized to judge the reconstruction performance. The RMS of the glass plate's phase distortion is about 0.62 μm. The RMS of the recovering residual error is about 0.11 μm. This value equals to about 1/10 λ. This value could meet the requirement of residual wavefront criterion for near-ideal CBC performance [8]. Fig. 5(c) also reveals that there exist high order aberrations which are beyond the capacity of the 7-element AFOC array wavefront sensor. Correction of external phase distortion mainly with low order aberrations is demonstrated here. Further promotion of the wavefront sensing abilities depends on increment of array scale and reduction of sub-aperture size.

Discrete structure decides that the fiber laser array's phase manipulation could only be operated within sub-apertures. Piston and tip/tilt errors are the most common aberrations that could be compensated. The former could be accomplished by devices like fiber-integrated phase modulator and piezoelectric-ring-based fiber phase modulator. Tip/tilt could be implemented by the AFOC devices. Higher order aberration modes, like defocus, astigmatism and so on, are hard to be corrected now. Here, we use the homemade piezoelectric-ring fiber phase modulator to pre-compensate the pistons. As shown in Fig. 6, sub-aperture averaged pistons calculated

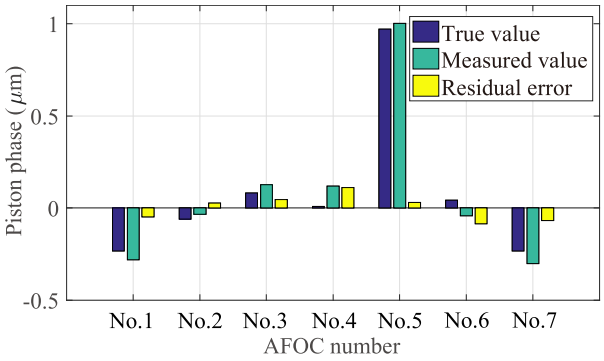

FIGURE 6. Sub-aperture averaged piston calculated from the wavefront profile shown in Fig. 5(b).

from the wavefront profile shown in Fig. 6. The central #5 AFOC is with the largest piston due to the major distortion of defocus. The max absolute value of the measured residual error is 0.10 λ and the mean Value is 0.055 λ, the RMS is 0.062 λ. Such detecting precision is enough for CBC applications.

Tip/tilt control here coexists in the wavefront reconstruction procedure. When the power of the coupled laser beacon in each of the AFOC is maximized, sub-aperture tip/tilt errors have been also corrected for both the laser beams' receiving and transmitting functions of the AFOC array [23], [24]. Sub-aperture wavefront slope vector measured results could reveal the tip/tilt correction performance to some extent. The results are shown in Fig. 7. Due to the central zone of defocus and astigmatism is centrally symmetric or flat, the measured sub-aperture tiled angles in the X-direction and Y-direction of the central AFOC (#5) are much less than the other AFOCs. RMS of absolute value of the tip/tilt measurement residual error is 0.22 λ/d and the mean value is 0.16 λ/d. Aberrations beyond tip/tilt located in the sub-aperture could decease the detecting precision and influence the correction results. Minimize the element size would promote the detecting and correcting abilities.

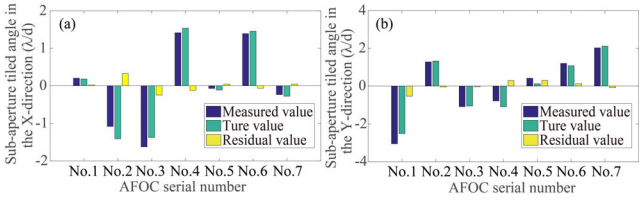

FIGURE 7. Measured sub-aperture tiled angle in the (a) X-direction and (b) Y-direction.

Fig. 8 shows the three dimensional long-exposure far-field patterns of the outgoing laser beams from the 7-element AFOC array in steps of ①, ② and ③. In step ①, alignment mechanical error induces noncoaxial deviation between the AFOC array element. Optical path difference results in random initial phase distribution of the fiber laser array. Both the two reasons lead to that the far-field pattern is flat and

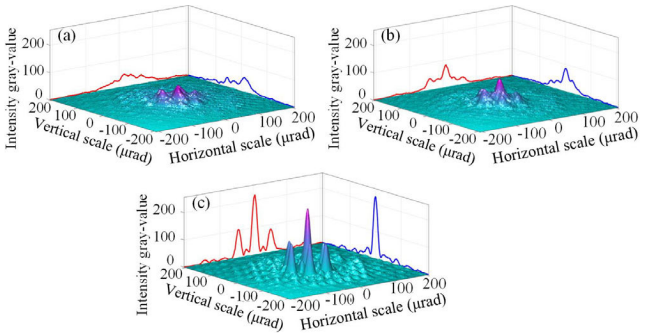

FIGURE 8. Far-field spot distribution during the calibration processors. (a) Correction in open loop; (b) Tip/tilt correction; (c) Pistons correction with SPGD.

without obvious coherent stripes, as shown in Fig. 8(a). After the sub-aperture tip/tilt errors are corrected, peak intensity is promoted slightly and the concentration of the intensity distribution is obviously increased in Fig. 8(b). After the pistons are eliminated, far-field pattern approximate to ideal CBC is formed and illustrated by Fig. 8(c). Six primary side lobes are obvious due to the limited array-filled-factor (0.875). When the array-filled-factor is less than 0.7, the 12 secondary side lobes become clearly visible in theory. Owning to the aberrations of high orders caused by the glass plate, there exist a lot of speckles in the background of the image. Meanwhile, Gaussian distribution outgoing beam from each single collimator (beam waist diameter $\omega_s = 23$ mm) is truncated by the sub-aperture diameter ($d = 28$ mm). The side lobes are more serious in consideration of larger beam truncation coefficient d/ω_s. The outgoing laser beams are phase-locked on the whole aperture pupil.

Fig. 9(a) illustrates the dispersion of the far-field combined spot captured in step ④. Such dispersion is caused by the phase distortion of the glass plate. The phase distortion could come from turbulence inducing aberrations and thermal blooming phenomenon in practical applications. Such outside aberrations may decrease CBC to non-CBC. When the tip/tilt errors distributed in each of the AFOC array are corrected in step ⑤, the combined spot performance is

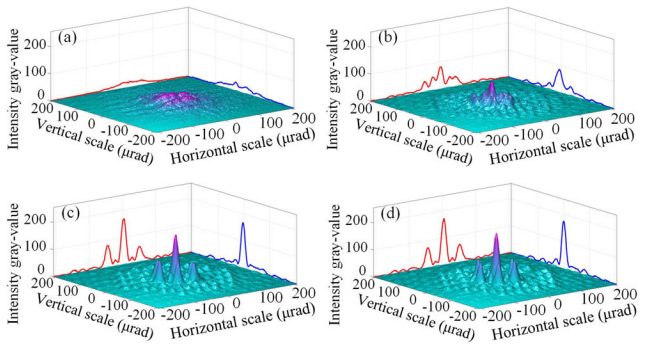

FIGURE 9. Far-field spot distribution during the pre-compensation processors. (a) Glass plate placed; (b) Tip/tilt correction; (c) Pistons pre-compensated; (d) Correction through SPGD.

improved, as shown in Fig. 9(b). Fig. 9(c) shows the combined spot obtained after the sub-aperture pistons is measured and pre-compensated in step ⑥. This pattern is very close to the ideal CBC far-field pattern of a 7-element fiber laser array. This proves that wavefront sensing and pre-compensation of the external aberrations of the AFOC array proposed in this paper is effective. To further confirm the correction performance and as a contrast, Fig. 9(d) presents the CBC results obtained through the most common SPGD control in step ⑦. This SPGD control is based on optimizing the far-field PIB metric through iterative calculation of the voltages applied on AFOCs and phase compensators, as described in part 3. It could be concluded that wavefront sensing and aberrations pre-compensation could obtain the same CBC performance in fiber laser array applications. The results shown in Fig. 8 and Fig. 9 are the average values of 20 trials.

The normalized PIB metrics located in circle with diameter of the whole aperture diffraction limit during the 7 experiment steps are shown in Fig. 10. The metrics are calculated from the seven far-field patterns shown in Fig. 8 and Fig. 9 and divided by the maximum value to be normalized. PIB gain factor about $0.74/0.21 = 3.5$ is obtained through active and aberrations pre-compensation based on wavefront sensing in step ⑥, compared with the value without correction in step ④. It should be noticed that the PIB of 0.74 in step ⑥ is lower than the PIB of 0.78 obtained through SPGD control in step ⑦. The reason is that some residual errors remain in the element-number-limited AFOC array. Meanwhile, both the two PIB value is lower than the maximum in step ③. This can be attributed to higher order aberrations that are beyond the abilities of the AFOC array. At the same time, absorption and scattering on the glass plate surfaces could also bring down the PIB metric.

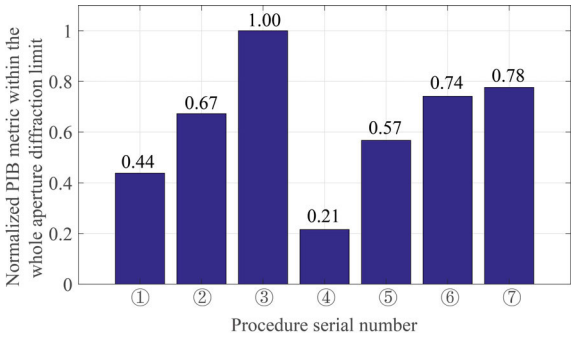

FIGURE 10. Normalized PIB metrics with circle size of whole aperture diffraction limit calculated from the far-field image.

The curve of the PIB metric obtained by the photo-detector (named as *PD-PIB*) during the experimental procedures is shown in Fig. 11. The metric is also divided by the maximum value to be normalized. The curves changing rules basically keep consistent with that illustrated in Fig. 8 and Fig. 9. There exists some difference between the PIB metric in step ⑥ (*PD-PIB* = 0.48) and step ⑦ (*PD-PIB* = 0.68)

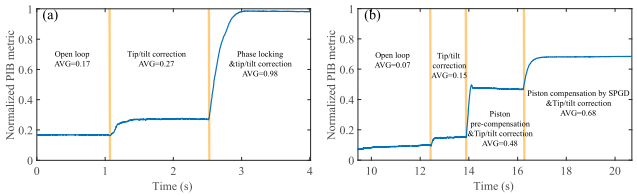

FIGURE 11. Experimental results of the PIB metric curve.

shown in Fig. 11(b). However, these two procedures' *PIB* values shown in Fig. 10 are very close and bigger (0.74 and 0.78 correspondingly). This could be explained by that fiber tip of the beacon laser and the detecting pinhole do not overlap with each other on the virtual focal plane. Actually, the position deviation between the two peak-value points shown in Fig. 9(c) and Fig. 9(d) is about 21.6 μm. Meanwhile, the pinhole used to get the PIB metric is with size of 20 μm, which is just about half of the whole aperture diffraction limit size of 42.3 μm. Therefore, the *PD-PIB* values are different from the values shown in Fig. 10.

V. CONCLUSION

A novel adaptive correcting method in the fiber laser array system is proposed and demonstrated through an experiment with a 7-element AFOC array. This method enables the fiber laser array based transceivers to pre-compensate the external aberrations, without limit of transmission delay and increment of array element. What is more, this method could integrate into the fiber laser array system without any additional complex spatial optical facilities. Such adaptive system could be utilized to pre-compensate the turbulence-induced aberrations located on the transmission path outside the array in applications like directed energy and free space laser communication. Experimental results verify the validity of such adaptive correction method. Such method would be further integrated with the internal phase noises correction techniques. This would be researched in the near future. However, such adaptive aberrations pre-compensating meets some difficulties when facing practical applications. Bandwidth of the tip/tilt correction should be fast enough to deal with the dynamic turbulence-induced aberrations. Actually, effective bandwidth approximating 100 Hz, which is also the characteristic frequency of the atmospheric turbulence, have already been achieved [32], [33]. Another difficulty is that the spatial frequency of the array system is limited to less than $1/d$ due to its unique structure. Smaller aperture size would help, but this will bring challenges to physical design.

REFERENCES

[1] Y. Yang, C. Geng, F. Li, G. Huang, and X. Li, "Multi-aperture all-fiber active coherent beam combining for free-space optical communication receivers," *Opt. Exp.*, vol. 25, no. 22, pp. 27519–27532, 2017.

[2] D. J. Geisler, T. M. Yarnall, M. L. Stevens, C. M. Schieler, B. S. Robinson, and S. A. Hamilton, "Multi-aperture digital coherent combining for free-space optical communication receivers," *Opt. Exp.*, vol. 24, no. 12, pp. 12661–12671, Jun. 2016.

[3] C. Geng, F. Li, J. Zuo, J. Liu, X. Yang, T. Yu, J. Jiang, and X. Li, "Fiber laser transceiving and wavefront aberration mitigation with adaptive distributed aperture array for free-space optical communications," *Opt. Lett.*, vol. 45, no. 7, pp. 1906–1909, Apr. 2020.

[4] C. Rao, S. Cui, Y. Tu, K. Zhou, and D. Liu, "Toward practical digital phase alignment for coherent beam combining in multi-aperture free space coherent optical receivers," *IEEE Access*, vol. 8, pp. 202585–202595, 2020.

[5] Y. Tu, S. Cui, K. Zhou, and D. Liu, "Phase alignment with minimum complexity for equal gain combining in multi-aperture free-space digital coherent optical communication receivers," *IEEE Photon. J.*, vol. 12, no. 2, pp. 1–10, Apr. 2020.

[6] Y. Ma, X. Wang, J. Leng, H. Xiao, X. Dong, J. Zhu, W. Du, P. Zhou, X. Xu, L. Si, Z. Liu, and Y. Zhao, "Coherent beam combination of 1.08 kW fiber amplifier array using single frequency dithering technique," *Opt. Lett.*, vol. 36, no. 6, pp. 951–953, Aug. 2011.

[7] M. A. Vorontsov and S. L. Lachinova, "Laser beam projection with adaptive array of fiber collimators. I. Basic considerations for analysis," *J. Opt. Soc. Amer. A, Opt. Image Sci.*, vol. 25, no. 8, pp. 1949–1959, Sep. 2008.

[8] S. L. Lachinova and M. A. Vorontsov, "Laser beam projection with adaptive array of fiber collimators. II. Analysis of atmospheric compensation efficiency," *J. Opt. Soc. Amer. A, Opt. Image Sci.*, vol. 25, no. 8, pp. 1960–1973, Sep. 2008.

[9] M. Vorontsov, G. Filimonov, V. Ovchinnikov, E. Polnau, S. Lachinova, T. Weyrauch, and J. Mangano, "Comparative efficiency analysis of fiber-array and conventional beam director systems in volume turbulence," *Appl. Opt.*, vol. 55, no. 15, pp. 4170–4185, May 2016.

[10] S. L. Lachinova and M. A. Vorontsov, "Performance analysis of an adaptive phase-locked tiled fiber array in atmospheric turbulence conditions," *Proc. SPIE*, vol. 5895, Aug. 2005, Art. no. 58950O.

[11] X. Wang, X. Wang, P. Zhou, R. Su, C. Geng, X. Li, X. Xu, and B. Shu, "350-W coherent beam combining of fiber amplifiers with tilt-tip and phase-locking control," *IEEE Photon. Technol. Lett.*, vol. 24, no. 19, pp. 1781–1784, Oct. 1, 2012.

[12] V. E. Leshchenko, "Coherent combining efficiency in tiled and filled aperture approaches," *Opt. Lett.*, vol. 23, no. 12, pp. 15944–15970, Jun. 2015.

[13] C. X. Yu, S. J. Augst, S. M. Redmond, K. C. Goldizen, D. V. Murphy, A. Sanchez, and T. Y. Fan, "Coherent combining of a 4 kW, eight-element fiber amplifier array," *Opt. Lett.*, vol. 36, no. 14, pp. 2686–2688, Jul. 2011.

[14] J. Zhu, P. Zhou, Y. Ma, X. Xu, and Z. Liu, "Power scaling analysis of tandem-pumped Yb-doped fiber lasers and amplifiers," *Opt. Exp.*, vol. 19, no. 19, pp. 18645–18654, Sep. 2011.

[15] V. I. Tatarskii, *Wave Propagation in a Turbulent Medium*. New York, NY, USA: McGraw-Hill, Jan. 1961.

[16] T. Weyrauch, M. A. Vorontsov, G. W. Carhart, L. A. Beresnev, A. P. Rostov, E. E. Polnau, and J. J. Liu, "Experimental demonstration of coherent beam combining over a 7 km propagation path," *Opt. Lett.*, vol. 36, no. 22, pp. 4455–4457, Nov. 2011.

[17] M. A. Vorontsov and V. P. Sivokon, "Stochastic parallel-gradient-descent technique for high-resolution wavefront phase-distortion correction," *J. Opt. Soc. Amer. A, Opt. Image Sci.*, vol. 15, no. 10, pp. 2745–2758, Oct. 1998.

[18] T. Weyrauch, M. Vorontsov, J. Mangano, V. Ovchinnikov, D. Bricker, E. Polnau, and A. Rostov, "Deep turbulence effects mitigation with coherent combining of 21 laser beams over 7 km," *Opt. Lett.*, vol. 41, no. 4, pp. 840–843, Feb. 2016.

[19] C. Geng, W. Luo, Y. Tan, H. Liu, J. Mu, and X. Li, "Experimental demonstration of using divergence cost-function in SPGD algorithm for coherent beam combining with tip/tilt control," *Opt. Exp.*, vol. 21, no. 21, pp. 25045–25055, Oct. 2013.

[20] D. Zhi, P. Ma, Y. Ma, X. Wang, P. Zhou, and L. Si, "Novel adaptive fiber-optics collimator for coherent beam combination," *Opt. Exp.*, vol. 22, no. 25, pp. 31520–31528, Dec. 2014.

[21] D. Zhi, Y. Ma, Z. Chen, X. Wang, P. Zhou, and L. Si, "Large deflection angle, high-power adaptive fiber optics collimator with preserved near-diffraction-limited beam quality," *Opt. Lett.*, vol. 41, no. 10, pp. 2217–2220, May 2016.

[22] F. Li, C. Geng, G. Huang, Y. Yang, and X. Li, "Wavefront sensing based on fiber coupling in adaptive fiber optics collimator array," *Opt. Exp.*, vol. 27, no. 6, pp. 8943–8957, Mar. 2019.

[23] F. Li, C. Geng, X. Li, and Q. Qiu, "Co-aperture transceiving of two combined beams based on adaptive fiber coupling control," *IEEE Photon. Technol. Lett.*, vol. 27, no. 17, pp. 1790–1797, Sep. 1, 2015.
[24] F. Li, C. Geng, G. Huang, Y. Yang, X. Li, and Q. Qiu, "Experimental demonstration of coherent combining with tip/tilt control based on adaptive space-to-fiber laser beam coupling," *IEEE Photon. J.*, vol. 9, no. 2, pp. 1–12, Apr. 2017.
[25] D. J. Bowman, M. J. King, A. J. Sutton, D. M. Wuchenich, R. L. Ward, E. A. Malikides, D. E. McClelland, and D. A. Shaddock, "Internally sensed optical phased array," *Opt. Lett.*, vol. 38, no. 7, pp. 1137–1139, Apr. 2013.
[26] L. E. Roberts, R. L. Ward, S. P. Francis, P. G. Sibley, R. Fleddermann, A. J. Sutton, C. Smith, D. E. McClelland, and D. A. Shaddock, "High power compatible internally sensed optical phased array," *Opt. Exp.*, vol. 24, no. 12, pp. 13467–13479, Jun. 2016.
[27] M. A. Vorontsov, S. L. Lachinova, L. A. Beresnev, and T. Weyrauch, "Obscuration-free pupil-plane phase locking of a coherent array of fiber collimators," *J. Opt. Soc. Amer. A, Opt. Image Sci.*, vol. 27, no. 11, pp. A106–A121, Nov. 2010.
[28] R. J. Noll, "Zernike polynomials and atmospheric turbulence," *J. Opt. Soc. Amer. A, Opt. Image Sci.*, vol. 66, no. 3, pp. 207–211, 1976.
[29] J. Hermann, "Cross coupling and aliasing in modal wave-front estimation," *J. Opt. Soc. Amer. A, Opt. Image Sci.*, vol. 71, no. 8, pp. 989–992, Aug. 1981.
[30] W. Luo, C. Geng, Y.-Y. Wu, Y. Tan, Q. Luo, H.-M. Liu, and X.-Y. Li, "Experimental demonstration of single-mode fiber coupling using adaptive fiber coupler," *Chin. Phys. B*, vol. 23, no. 1, Jan. 2014, Art. no. 014207.
[31] H. Takenaka, M. Toyoshima, and Y. Takayama, "Experimental verification of fiber-coupling efficiency for satellite-to-ground atmospheric laser downlinks," *Opt. Exp.*, vol. 20, no. 14, pp. 15301–15308, Jul. 2012.
[32] G. Huang, C. Geng, F. Li, J. Liu, and X. Li, "Control bandwidth promotion of adaptive fiber-optics collimator and its application in coherent beam combination," *IEEE Photon. J.*, vol. 10, no. 6, pp. 1–13, Dec. 2018.
[33] G. Huang, C. Geng, F. Li, Y. Yang, and X. Li, "Adaptive SMF coupling based on precise-delayed SPGD algorithm and its application in free space optical communication," *IEEE Photon. J.*, vol. 10, no. 3, pp. 1–12, Jun. 2018.

CHAO GENG was born in Anhui, China, in 1984. He received the bachelor's degree in optic-information science and technology from the Huazhong University of Science and Technology (HUST), in 2006, and the Ph.D. degree in optical engineering from the Graduate School of Chinese Academy of Sciences (CAS), in 2011.

In July 2011, he was employed as an Assistant Professor with the Key Laboratory on Adaptive Optics, Institute of Optics and Electronics (IOE), CAS. In 2018, he has engaged as a Doctoral Supervisor in optical engineering with the University of Chinese Academy of Sciences. Since December 2014, he has been an Associate Professor with IOE, CAS. Since 2015, he has also been a member of the Youth Innovation Promotion Association of CAS. Related research works were published by over 40 articles, ten Chinese invention patents, and a coauthored monograph entitled "Adaptive Stochastic Parallel Optimized Control Technology and Its Application." His main research interests include the research of fiber laser applications and adaptive optics, to explore and figure out key scientific and technical issues about how adaptive fiber-optic distributed aperture array works in laser transmission and FSOC.

FAN ZOU received the B.S. degree in pharmacy from Fudan University, Shanghai, China, in 2017. He is currently pursuing the M.S. degree in optics with the Institute of Optics and Electronics, Chengdu, China.

FENG LI received the Ph.D. degree from the School of Optoelectronic Information, University of Electronic Science and Technology of China, Chengdu, China. He is currently an Associate Research Fellow with the Institute of Optics and Electronics, Chinese Academy of Sciences. His current research interests include adaptive optics and free space fiber laser communications.

GUAN HUANG was born in Tongchuan, Shannxi, China, in 1992. He received the B.S. degree from Shandong University, and the Ph.D. degree from the University of Chinese Academy of Sciences, Beijing, China, in 2019.

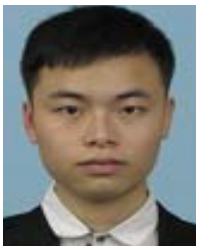

JING ZUO received the B.S. degree from Yangtze University, in 2017. He is currently pursuing the Ph.D. degree in optics with the Institute of Optics and Electronics, Chengdu, China.

JIAYING LIU was born in Henan, China, in 1995. She received the B.S. degree in optical information science and technology and the B.S. degree in communication engineering from the Nanjing University of Posts and Telecommunications, Nanjing, China, in 2016. She is currently pursuing the Ph.D. degree in optical engineering with the Institute of Optics and Electronics, Chinese Academy of Sciences. Her research interests include the optical communication, optical combination in fiber device, and laser transmission with atmospheric turbulence.

ZHIHUA FAN was born in Sichuan, China, in 1981. He received the bachelor's degree in mechanical design manufacture and automation from Sichuan University (SCU), in 2006, and the Ph.D. degree in signal and information processing from the Graduate School of Chinese Academy of Science (CAS), in 2011.

In July 2011, he was employed as an Engineer with the Shanghai Institute of Spaceflight Control Technology (SISCT), Shanghai Academy of Spaceflight Technology, China Aerospace Science and Technology Corporation (CASC). From 2015 to 2020, he was an Academic Secretary of the Infrared Detection Technology Research and Development Center, CASC. Since August 2013, he has been a Senior Engineer with SISCT, CASC. He is currently an Associate Professor with the Sichuan University of Arts and Science. He has authored more than 15 articles, and more than 12 Chinese invention patents. His research interests include photoelectric detection applications, adaptive optics, and laser applications.

XINYANG LI received the bachelor's degree in automatic control and mechanics from Shanghai Jiao Tong University (SJTU), in 1993, and the master's and Ph.D. degrees in optical engineering from the Institute of Optics and Electronics (IOE), Chinese Academy of Sciences (CAS), in 1997 and 2000, respectively.

He is currently a Professor and the Deputy Director of the Laboratory on Adaptive Optics, IOE, and a Professor with the University of Chinese Academy of Sciences (UCAS). He has been responsible for the design, development, and test of several adaptive optics systems. He has a high attainment, especially in the engineering practice of laser propagation in atmosphere and adaptive optics correction technology. He has published more than 300 papers in academic journals and conferences, and has received more than 30 authorized invention patents. His research interests include optical engineering, adaptive optics, atmospheric optics, laser technology, laser communication technology, and so on. He is a member of the Chinese Optical Society (COS), the Chinese Society for optical Engineering (CSOE), the International Society for Optical Engineering (SPIE), and the Optical Society of America (OSA). He has won the Second Prize of National Science and Technology Invention, the First Prize of Science and Technology Progress of CAS, and the Collective Prize of the Excellent Science and Technology Achievement Award of CAS.